Surrogate-Based Optimization Applied to Benchmark Aerodynamic Design Problems

Conference Paper · June 2017

DOI: 10.2514/6.2017-4367

3 authors:

Yu Zhang

15 PUBLICATIONS **545** CITATIONS

SEE PROFILE

Zhong-Hua Han

Northwestern Polytechnical University

146 PUBLICATIONS **2,870** CITATIONS

SEE PROFILE

Leifur Leifsson

Iowa State University

226 PUBLICATIONS **2,341** CITATIONS

SEE PROFILE

AIAA SciTech
4-8 January 2016, San Diego, California, USA
54th AIAA Aerospace Sciences Meeting

Multi-round Surrogate-based Optimization for Benchmark Aerodynamic Design Problems

Yu Zhang[1], Zhong-Hua Han[2]*, Lai-Xiang Shi[3] and Wen-Ping Song[4]
National Key Laboratory of Science and Technology on Aerodynamic Design and Research, School of Aeronautics, Northwestern Polytechnical University, Xi'an, 710072, P. R. China

Two benchmark problems provided by AIAA aerodynamic design optimization discussion group (ADODG) are performed using an in-house surrogate-based optimizer called "SurroOpt". One is drag minimization of the NACA 0012 in transonic inviscid flow and the other is drag minimization of the RAE 2822 in transonic viscous flow. A so-called "multi-round optimization strategy" is used to find the global optimal solution. In each round, surrogate models are constructed both for the objective function and constraints, and the infill-sampling criterion, maximizing constrained expected improvement (EI) is adopted to refine the models. Especially, the design space in each round is adjusted on the basis of the optimal airfoil of previous round. In addition, not only the optimal airfoil, but also a part of samples of previous round are also taken as initial samples of the next round to speed up the process of the optimization. The airfoils are parameterized by the class-shape function transformation (CST) method and an in-house CFD code called "PMNS2D" is used to solve the compressible Euler and Reynolds-averaged Navier-Stokes equations. The results show that the design space has great influence on the result of the optimization and the drag coefficients of airfoils are reduced dramatically via transforming the design space. This multi-round optimization strategy turns out to be efficient and suitable for surrogate-based optimization. The optimizations based on different dimensions of design space are also studied. For the NACA0012 case, as the dimension increases, the result of optimization improves until a limit value is reached, while more computational costs are required; however, the result indicates that the RAE2822 case is insensitive to the dimensions.

Nomenclature

Area	=	area of the airfoil
C_l	=	lift coefficient
C_d	=	drag coefficient
C_m	=	moment coefficient
c	=	chord length of the airfoil
Ma	=	Mach number of the flow
Re	=	Reynolds number of the flow

I. Introduction

Over past three decades, computational fluid dynamics (CFD) has been highly developed, while the CFD-driven aerodynamic design optimization (ADO) also matures to a stage that it has been used in aircraft design and

1 Master candidate, P.O. Box754, Northwestern Polytechnical University, Youyi West Road, No. 127; 465553039@qq.com.
2 Professor, P.O. Box 754, Northwestern Polytechnical University, Youyi West Road, No. 127; hanzh@nwpu.edu.cn; AIAA member.
3 Master candidate, P.O. Box754, Northwestern Polytechnical University, Youyi West Road, No. 127; 345335197@qq.com.
4 Professor, P.O. Box 754, Northwestern Polytechnical University, Youyi West Road, No. 127; wpsong@nwpu.edu.cn.

plays an increasing role in improving the performance. The CFD-driven ADO can be divided into two classes: direct optimization and surrogate-based optimization (SBO). The direct optimization method mainly refers to the gradient-based method or evolutionary algorithms (EA) such as genetic algorithms (GAs). The gradient-based method has been proven to be every effective [1][2][3] when gradients are computed by the adjoint method[4][5]. However, it's a local optimization method and effected greatly by the initial design. Especially in ADO, the design space is typically multidimensional, nonlinear with multi-peak values. GAs based optimization is a global optimization method which can find the globally optima. However, it needs a large amount of CFD evaluations, particularly when high-fidelity CFD is adopted. For this reasons, the SBO method is introduced in ADO, and has turned out to have great potentials.

Recently, SBO has made great advance [6][7][8]. SBO denotes a type of numerical optimization method which makes use of surrogate models to guide the search of new design which is mostly likely to the optimum. First the surrogate model are constructed for the objectives and constraints, based on the samples selected by DoE[9][10] and evaluate by high-fidelity numerical simulation. Then the model is repetitively refined by adding new sample point selected by infill-sampling criteria [11] such as maximizing the expected improvement (EI)[12]. Once the surrogate model is constructed, the expensive CFD is replaced by the predictions of surrogate models and the high-fidelity CFD is only needed in the evaluation of new samples. With the increasing of iterations, the surrogate model is more accurate and the optimization is convergent to the optimal solution. It has been shown that SBO method [13] can remarkably improve the efficiency of optimization [6][14][15], and has the capability of finding global optima[12]. Forrester reviewed the state of the art of constructing surrogate models and their use in optimization strategies in 2009[13]. And the surrogate models were classified into six strategies: polynomials or response surface model[16], moving least-squares (MLS)[17], radial based functions (RBFs)[18], kriging[19][20][21], support vector regression (SVR)[22][23] and some new developed models enhanced with additional design information, such as gradient enhanced model[24][25] and variable-fidelity model[26][27][28]. The infill criteria were divided into four types: 1) the exploitation including minimizing the predictor and trust region method[29]; 2) the exploration such as maxi-min criterion infilling the samples at the position with maximum estimated error; 3) the balanced exploitation/exploration including two-stage approaches, such as statistical lower confidence bound(LCB), probability of improvement(PI) and expected improvement (EI)[12], and one-stage approaches, such as goal seeking [30] giving a suitable value for global optimum and searching for a specific improvement and the conditional LCB method; 4) parallel infill criteria which obtains a number of infill samples by using infill criteria simultaneously. Since kriging can represent high nonlinear functions while offering error estimation and EI has been proven to be very efficient to finding the global optimization, the kriging combined with EI method is widely used in ADO[13][31][32].

Another issue about ADO is how to determine the design space. As we can see, the design space of ADO is complex, and highly related to the geometric parameterization method. For most of the parameterization methods, the coefficients or design variables are coupled with each other. Consequently, different combination of design variables can result in airfoils which are very much close to each other. To obtain the optimal result, it seems like the design space should be as large as possible. However, it causes the optimization quite difficult. To address this issue, this paper comes up with a multi-round optimization strategy to work out this problem.

The AIAA aerodynamic design optimization discussion group (ADODG) has established a series benchmark problem of increasingly complex which are suitable for exercising aerodynamic optimization methods in a constrained design space. It can be used to comparative evaluation for different optimization methods. In this paper, we are trying to find the global optimal solution via surrogate-based optimization (SBO) and we highlight the specific strategies employed in this work are multi-round optimization and local optimization method. Two 2-d benchmark problems are addressed: (1) the drag minimization of the NACA 0012 airfoil in transonic inviscid flow; (2) the drag minimization of the RAE 2822 airfoil in transonic viscous flow. The class-shape function transformation (CST) method [33] is employed in this paper. The grid convergence studies for initial and optimal airfoil are presented and the impact of the dimensionality is also studied, as requested by ADODG.

II. Methodology

A. Shape Parameterization Method

The CST method [33] is adopted to parameterize the airfoils. Its mathematical expression is

$$
\begin{aligned}
&y(x) = C_{N2}^{N1}(x)\cdot S(x) + x\cdot \mathrm{y_{TE}}, \qquad \mathrm{y_{TE}} = \Delta \mathrm{y_{TE}}/c \\
&C_{N2}^{N1}(x) = x^{N_1}(1-\mathrm{x})^{N_2} \\
&S(x) = \sum_{i=0}^{p} A_i B_{i,p}(x), \mathrm{S(0)} = \sqrt{2R_{\mathrm{LE}}/C}, \mathrm{S(1)} = \tan\beta + \Delta y_{\mathrm{TE}}/C
\end{aligned} \tag{1}
$$

Where the term $C_{N2}^{N1}(x)$ represents the "class function" which is used to define general classes of geometries and the term $S(x)$ is the "shape function" which is used to define specific shapes within the geometric class. Especially $S(0)$ is directly related to the normalized airfoil leading-edge nose radius R_{LE} and $S(1)$ is directly related to the airfoil boat-tail angle β and normalized trailing-edge thickness Δy_{TE} .

We set the class function exponents $N_1 = 0.5$ and $N_2 = 1.0$ to define the round nose and pointed-aft-end-typed airfoil. In fact the shape function is represented by summing up of the Bernstein polynomials, so their coefficients, A_i, serve as the design variables of our airfoil design problem.

B. The flower solver

An in-house CFD code called "PMNS2D"[34][35] is used to solve the compressible Euler or Reynolds-averaged Navier-Stokes equations. Jameson's central scheme is used for spatial discretization; for inviscid simulation, Runge-Kutta is used for time integration, whereas for viscous simulation, LU-SGS method is used. Multigrid, local-time stepping and variable-coefficient implicit residual smoothing are utilized to accelerate the solution converging to steady state. Particularly for the benchmark test case 1 (inviscid simulation of a modified NACA 0012 airfoil in transonic flow), single grid is used, since the using of multigrid technique can frequently leads to non-zero lift at zero angle of attack; enthalpy dumping technique is also used, which greatly improves the efficiency and robustness of CFD simulation for case 1. For RANS simulations, Spalart-Allmaras turbulence model is used for turbulence closure.

The O-type grids for inviscid flow simulation are generated by solving elliptic equations with very good uniformity and orthogonality. The typical grids used for optimization have 320 points in the stream-wise direction and 160 points in the direction normal to the airfoil surface. The grid points were clustered at the trailing edge and the leading edge of the airfoil to give a minimum stream-wise spacing of 0.0005 × chord length; the normal spacing of the first grid line is around 0.0005 × chord length. The mesh has around 51,200 cells. Since a study on the influence of farfield distance on the drag coefficient shows that the drag coefficient doesn't change when farfield distance is larger than 140 chord length in Table 1, during the optimization, the farfield distance is set as 140 chord lengths. The flow simulation is terminated after the density residual has dropped 6 orders in magnitude or the maximum number of iteration of 5000 has been reached. A typical evaluation time of the inviscid CFD simulation (including grid generation and the flow solution) is around 3 minutes for a typical personal computer.

Table 1. Grid convergence study for NACA0012 airfoil w.r.t. farfield distance

Farfield distance(c)	C_l (cts)	C_d (cts)
20	0.0	475.31
40	0.0	481.56
60	0.0	482.19
80	0.0	482.56
100	0.0	482.08
120	0.0	482.85
140	0.0	483.03
160	0.0	483.12

The C-type grids for viscous flow simulation are generated using a special technique called conformal transformation which ensures very good uniformity and orthogonality. The typical grids used for optimization have 512 points in the stream-wise direction and 256 points in the direction normal to the airfoil surface. The grid points were clustered at the trailing edge and the leading edge of the airfoil to give a minimum stream-wise spacing of 0.00005 × chord length; the normal spacing of the first grid line away from the airfoil surface is set to ensure that it's $y^+<1$. The mesh has around 131,841 cells. Also a study on the influence of farfield distance on the drag coefficient shows that the drag coefficient doesn't change when farfield distance is larger than 90 chord length in Table 2, during the optimization,

the farfield distance is set as about 90 chord lengths. The flow simulation is terminated after the density residual has dropped 5.5 orders in magnitude or the maximum number of iteration of 10,000 has been reached. A typical evaluation time of the viscous CFD simulation (including grid generation and the flow solution) is around 1 hour for a typical personal computer.

Table 2. Grid convergence study for RAE 2822 airfoil w.r.t. farfield distance

Farfield distance(c)	C_l (cts)	C_d (cts)
30	82.31	191.63
60	82.37	192.07
90	82.39	191.83
120	82.40	191.76
150	82.40	191.79
180	82.40	191.68

C. Optimization Methodology

A surrogate-based multi-round optimization strategy is adopted to explore the global optimum of airfoil design problems. Figure 1 shows the framework of this method, and the essence of this method is that the design space in each round is adjusted on the basis of the optimal airfoil of previous round; meanwhile the optimal airfoil of previous round is taken as one of the initial samples of the next round; in addition, a part of samples of previous round are also taken as initial samples of the next round to speed up the process of the optimization and save the computational cost.

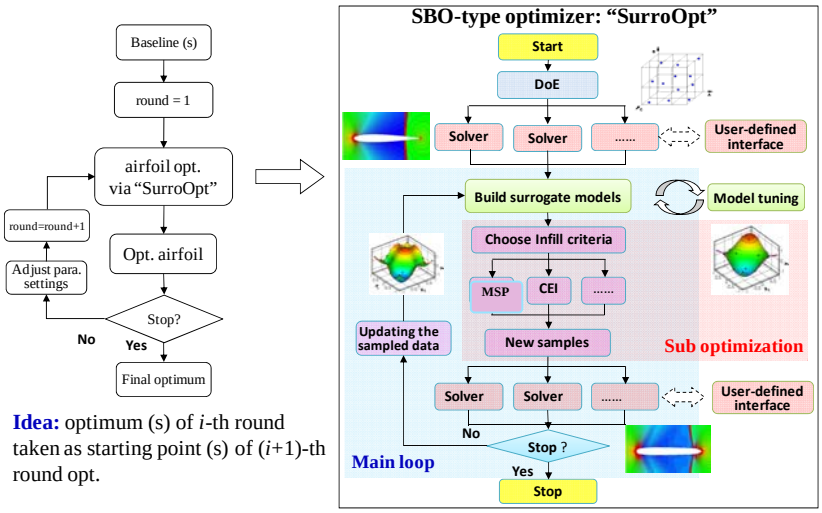

Figure 1. Framework of airfoil design via a SBO-type optimizer (left: the main loop of multi-round optimization; right: the flowchart of "SurroOpt").

An in-house optimization platform named "SurroOpt" is used in each round. After setting the design space, the initial samples are generated by design of experiments (DoE)[9][10]. "SurroOpt" offers functionality of Latin hypercube sampling (LHS)， uniform design (UD) and Monte Carlo design (MC), and we use Latin hypercube sampling (LHS) here. Then the samples are evaluated by CFD analysis. After that, the surrogate models can be constructed both for the objective functions and the constraints. There are different surrogate models such as quadratic response surface model (PRSM), kriging, gradient-enhanced kriging (GEK), hierarchical kriging (HK)[27], radial-basis functions (RBFs) available in "SurroOpt". Here kriging model is constructed in this study. Then the kriging models are refined by adding new points selected by specified infill criteria. "SurroOpt" mainly provides five infill sampling criteria, such as minimizing surrogate prediction (MSP), and minimizing lower confidence bounding (LCB), maximizing expected improvement (EI), maximizing probability of improvement (PI), and maximizing mean squared error (MSE). In our study, the infill criterion refers to maximizing the constrained expected improvement (EI). This criterion assumes that there is a normal distribution at each site; meanwhile the response and the mean squared error predicted by surrogate model serve as the mean value and the standard

deviation. So EI is defined as the mathematical expectation of improvement compared to the optimal solution observed so far. We get the maximum EI position by combining GA with local optimization, such as Hooke and Jeeves pattern search, quasi Newton's methods (BFGS) and sequential quadratic programming (SQP).

And the iteration terminated condition is

$$\left\| x^{(i+1)} - x^{(i)} \right\| < \varepsilon_1 \text{ or } N \geq N_{\max} \tag{2}$$

Where N_{max} is the user-specified maximal number of CFD evaluations, and $\varepsilon_1 = 1e-10$. When there is no new sample can be found or the number of samples reaches the maximum, a round of optimization terminates.

III. Benchmark Case I: Drag Minimization of the NACA 0012 in Transonic Inviscid Flow

A. Problem Statement

The optimization problem of this work is the drag minimization of a modified NACA0012 airfoil at a freestream Mach number of 0.85 at a zero angle of attack, subject to a full thickness constraint. It can be written as a standard nonlinear programming problem

$$\begin{aligned} &\min \ C_d \\ &s.t. \quad C_l = 0.0 \\ &\qquad y \geq y_{\text{baseline}} \quad \forall x \in [0,1]. \end{aligned} \tag{3}$$

The modified NACA0012 airfoil with zero thickness trailing edge is defined as

$$y_{baseline} = \pm 0.6\left(0.2969\sqrt{x} - 0.1260x - 0.3516x^2 + 0.2843x^3 - 0.1036x^4\right). \tag{4}$$

B. Grid Convergence Study for Initial Airfoil

The grid study for NACA0012 airfoil uses an in-house mesh generator by solving elliptic equations. Table 3 shows the grid study with respect to grid size for the initial airfoil NACA 0012. First, the grid study with respect to farfield distance is completed which shows that 140 chord lengths is a suitable farfield distance. So the grids in grid size study are all set as 140 chords away from the airfoil surface. It is observed that the lift coefficients of NACA0012 is all approximately equal to zero and the difference in drag coefficients is converging within 0.1 counts gradually with the increase of the number of cells.

Table 3. Grid convergence study for the NACA0012 w.r.t. grid size

Grid size	C_l (cts)	C_d (cts)
128 × 64	0.0	462.70
192 × 96	0.0	478.92
256 × 128	0.0	480.20
320 × 160	0.0	481.28
384 × 192	0.0	482.32
448 × 224	0.0	482.85
512 × 256	0.0	483.13
576 × 288	0.0	483.21

C. Results

A detailed process of optimization with 17 variables is depicted here. The optimization processes with different number of design variables are similar, and the impact of dimensionality is presented in the next subsection.

Since NACA0012 airfoil is the baseline airfoil, we get the initial parameters by parameterizing the NACA 0012. Then the design space is appropriately enlarged to explore the problem for the first round. The optimization is repeated three times in each round to ensure that it finds the optimal airfoil as much as possible. Figure 2 shows the initial design space in the first round obtained by expanding the parameters 1.5 times and narrowing it by half, and the optimal airfoils (the best one in three times) of optimization with different number of design variables in the first

round is also presented. Figure 3 shows the convergent histories of the optimizations and the comparisons of the pressure coefficient distributions between the NACA0012 and the optimal airfoil.

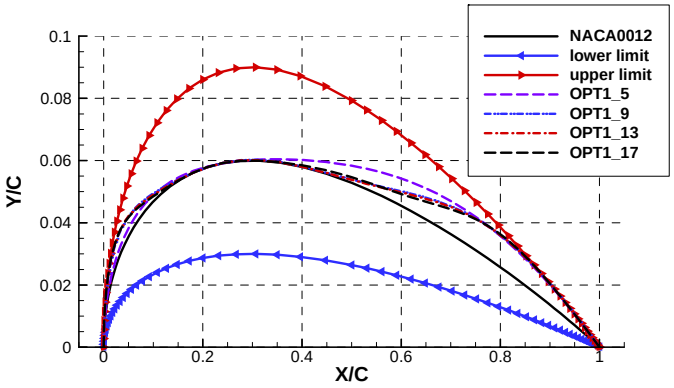

Figure 2. The initial design space and optimal airfoils in the first round for NACA0012 case.

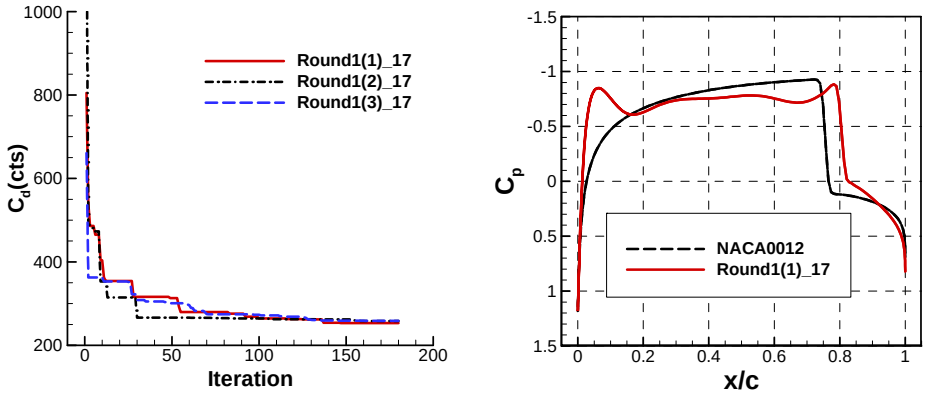

Figure 3. (left) Convergent histories and (right) comparison of pressure coefficient distributions for the baseline and optimal airfoils in the first round for NACA0012 case.

It is observed that still a strong normal shock exists from the pressure distribution or the pressure contour. Fortunately, we can clearly see that the leading edge and the trailing edge of optimal airfoils in optimization with different number of design variables are all reaching the upper limit of the design space in Figure 2, which means that better airfoil can exist out of the initial design space. However, when the design space gets further enlarged, it is more likely to come into a lot of odd airfoils which makes the optimization difficult to carry out. So we change the design space on the basis of the optimal airfoil of the first round by enlarging the range for the parameters that reach the boundary and reducing the range for the parameters which are within the boundary to carry on a new-round optimization. Particularly we enlarge the scope of the last parameter of CST which is corresponding to the airfoil boat-tail angle.

The multi-round optimization is conducted until all of the design variables of optimal airfoil are within the design space in the fourth round. So far, the optimization method is based on kriging model and combined with EI infilling criterion, which can be regard as a global optimization in current design space of each round. To guarantee that the optimization is full converged, an addition local optimization is conducted further, which is the fifth-round optimization. The shape and the pressure coefficient distribution of the optimal airfoil in each round are shown in Figure 4 and Figure 5. We can see that the latter part of the optimal airfoil is much thicker than the original airfoil which leads to a smooth upper surface in favor of reducing shock wave drag. Particularly there is a small bump existing in the chord-wise position of 0.7c to 0.8c of the optimal airfoil which can contribute to control the strength of the shock near the trailing edge.

The force coefficient of the optimal airfoil in each round is shown in Table 4. Figure 6 shows the process of the drag coefficient reduction in the multi-round optimization. As we can see, the decrease of drag coefficient is slowing down which means the optimization converges. The comparison of Mach number contours for baseline and final optimal airfoils are shown in Figure 7. It is clearly shown that the strongly shock wave on the NACA 0012 airfoil

surface is broken into an attached shock wave and a detached shock wave. Since the attached shock wave is much weaker, the shock wave drag is greatly reduced.

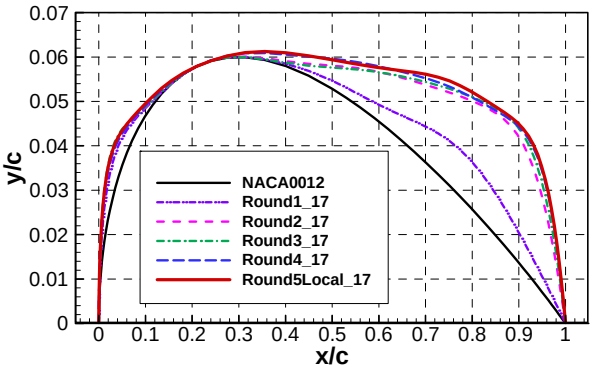

Figure 4. Shape of optimal airfoils in each round of optimization with 17 design variables (NACA 0012 airfoil test case)

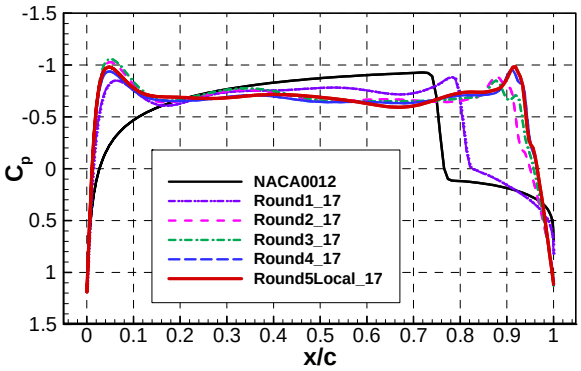

Figure 5. Pressure coefficient distributions of optimal airfoils in each round with 17 design variables (NACA 0012 airfoil test case)

Table 4. Force coefficients of optimal airfoil in each round with 17 design variables (NACA 0012 airfoil test case)

Variable	Baseline	1st round Opt.	2nd round Opt.	3rd round Opt.	4th round Opt.	5th round Opt.
C_l (cts)	0.0	0.0	0.0	0.0	0.0	0.0
C_d (cts)	481.28	253.52	95.24	86.42	74.70	73.08
N_CFD	/	167	184	206	275	100

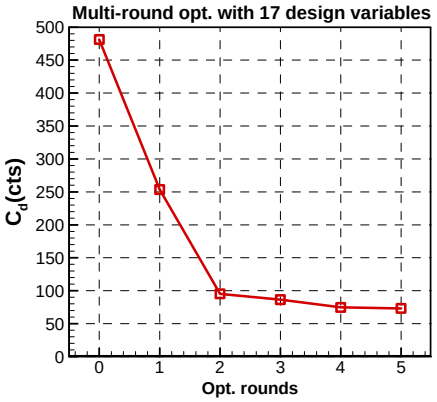

Figure 6. Convergent history of drag coefficient in multi-round optimization with 17 design variables (NACA 0012 airfoil test case)

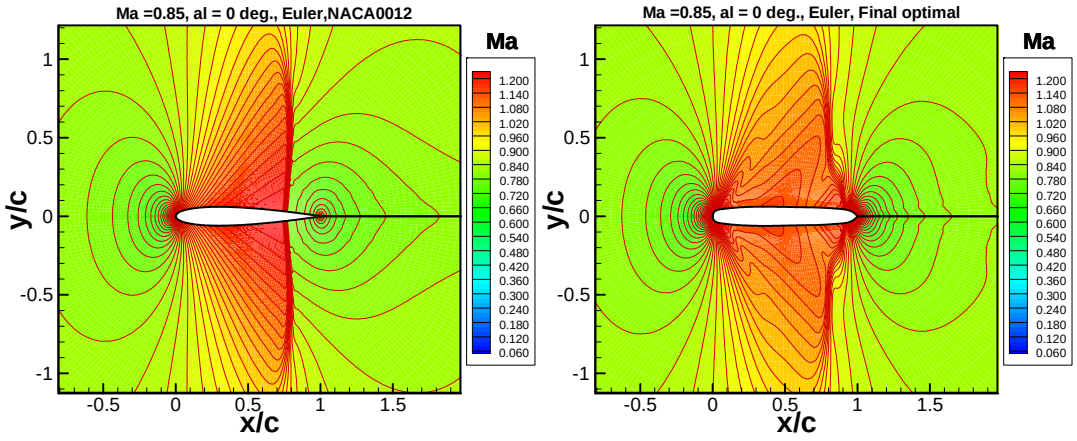

Figure 7. Comparison of Mach number contours of baseline and final optimal airfoils (NACA 0012 airfoil test case)

D. Grid Convergence Study for the Optimum Airfoil

The grid study for the final optimal airfoil is presented in Table 5. The farfield distance is set as 140 chord length away from the airfoil surface. It is shown that both the difference of lift and drag coefficients converge to 1 counts with the increase of the number of grid cells. As we mentioned before, the grids generated by solving elliptic equations has very good quality of uniformity and orthogonality, which makes the computation very robust and force coefficients convergent very quickly.

Table 5. Grid convergence study for the optimum airfoil with PMNS2D.

Grid size	C_l (cts)	C_d (cts)
320 × 160	0.0	73.08
384 × 192	0.0	69.81
448 × 224	0.0	68.28
512 × 256	0.0	67.50
576 × 288	0.0	66.82
640 × 320	0.0	66.48

E. Impact of Dimensionality of Design Space

To study the impact of the dimensionality on the optimization results as well as the computational costs, we set the order of the parameterization as 4, 8, 12, 16 (for CST parameterization), and the actual number of design variables is 5, 9, 13, 17, since the airfoils are enforced symmetrical during the optimization process. The same methodology has been applied for the optimization with different number of design variables. The processes of optimization are not specifically described, but the optimal airfoil and its pressure distribution in each round is demonstrated here.

For the optimization with 5 design variables, the shape and the pressure distribution of the optimal airfoil in each round is shown in Figure 8 and Figure 9. And the force coefficient of the optimal airfoil in each round is shown in Table 6. Specially, the local optimization with 5 design variables did not find a better design than global optimization, so it is terminates after the fourth global optimization round. For the optimization with 9 design variables, the shape and the pressure distribution of the optimal airfoil in each round is shown in Figure 10 and Figure 11. And the force coefficient of the optimal airfoil in each round is shown in Table 7. For the optimization with 13 design variables, the shape and the pressure distribution of the optimal airfoil in each round is shown in Figure 12 and Figure 13. And the force coefficient of the optimal airfoil in each round is shown in Table 8. Note that the results of the optimization with 17 design variables have been shown in part III.C.

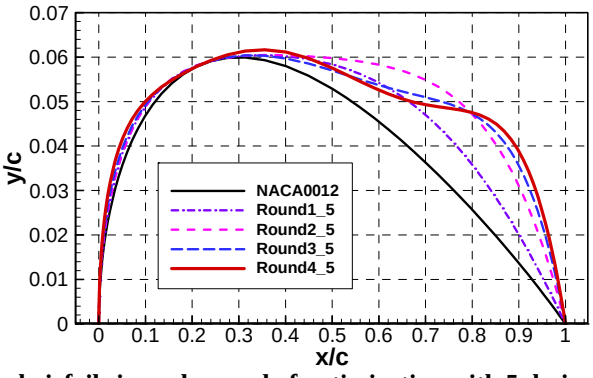

Figure 8. Shape of optimal airfoils in each round of optimization with 5 design variables (NACA 0012 airfoil test case)

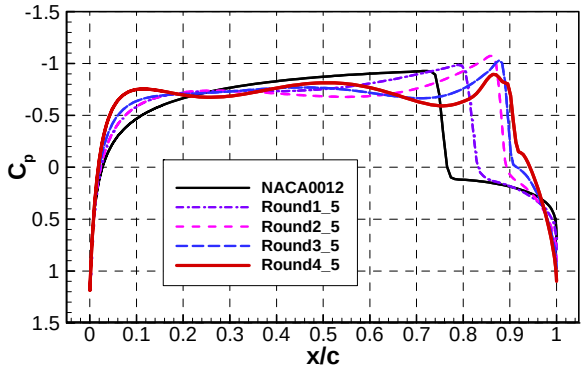

Figure 9. Pressure coefficient distributions of optimal airfoils in each round with 5 design variables (NACA 0012 airfoil test case)

Table 6. Force coefficient of optimal airfoil in each round of optimization with 5 design variables (NACA 0012 airfoil test case)

Variable	Baseline	1st round Opt.	2nd round Opt.	3rd round Opt.	4th round Opt.
C_l (cts)	0.0	0.0	0.0	0.0	0.0
C_d (cts)	481.28	377.08	301.92	214.11	174.29
N_CFD	/	35	67	104	163

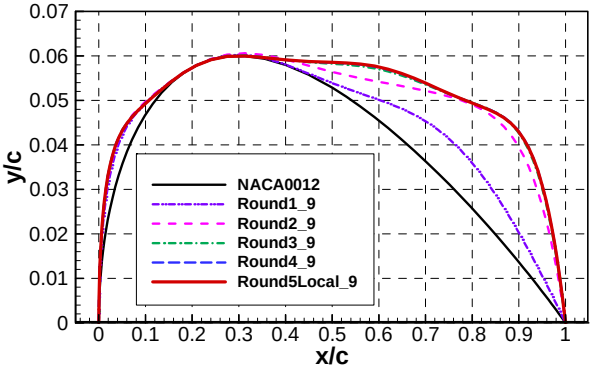

Figure 10. Shape of optimal airfoils in each round of optimization with 9 design variables (NACA 0012 airfoil test case)

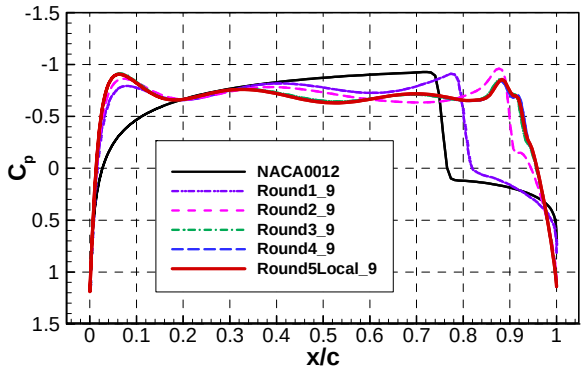

Figure 11. Pressure coefficient distributions of optimal airfoils in each round with 9 design variables (NACA 0012 airfoil test case)

Table 7. Force coefficient of optimal airfoil in each round of optimization with 9 design variables (NACA 0012 airfoil test case)

Variable	Baseline	1st round Opt.	2nd round Opt.	3rd round Opt.	4th round Opt.	5th round Opt.
C_l (cts)	0.0	0.0	0.0	0.0	0.0	0.0
C_d (cts)	481.28	279.27	128.62	95.49	93.15	92.75
N_CFD	/	138	186	256	149	77

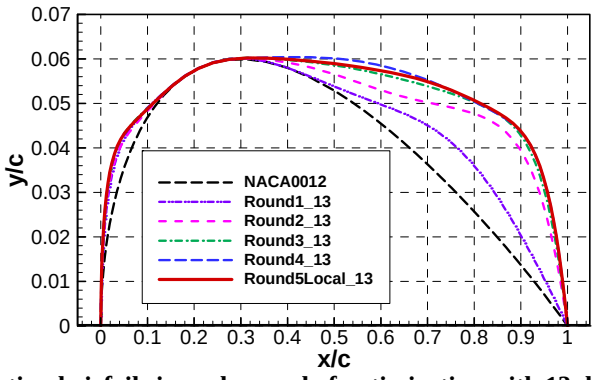

Figure 12. Shape of optimal airfoils in each round of optimization with 13 design variables (NACA 0012 airfoil test case)

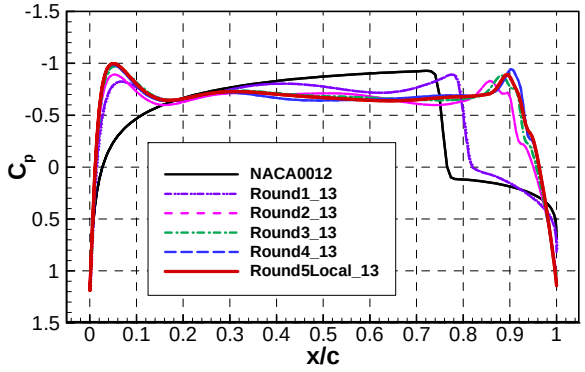

Figure 13. Pressure coefficient distributions of optimal airfoils in each round with 13 design variables (NACA 0012 airfoil test case)

Table 8. Force coefficient of optimal airfoil in each round of optimization with 13 design variables (NACA 0012 airfoil test case)

Variable	Baseline	1st round Opt.	2nd round Opt.	3rd round Opt.	4th round Opt.	5th round Opt.
C_l (cts)	0.0	0.0	0.0	0.0	0.0	0.0
C_d (cts)	481.28	263.88	110.20	87.69	79.78	75.32
N_CFD	/	111	104	126	292	162

Figure 14 (left) shows the comparison of convergence histories with varying number of design variables in the multi-round optimization. Table 9 and Figure 14 (right) shows the comparison of the final optimum results with different number of design variables. We could see that the convergence process of each optimization is similar and converges to a limit value, and the more variables, the optimization converges faster. However, the speed of optimization doesn't increase all the way, when the number of design variables increases to some extent, the speed of optimization is also reach a limit. As the dimension of the design space increases, the result of optimization improves until a limit value is reached. Note that the computational cost of CFD calls also continuously increases, but is not so much as expected. Based on the results above, we can come to the conclusion that the number of design variables does have dramatic influence on the optimization results, and at least 13 design variables is needed for this test case when CST method is employed.

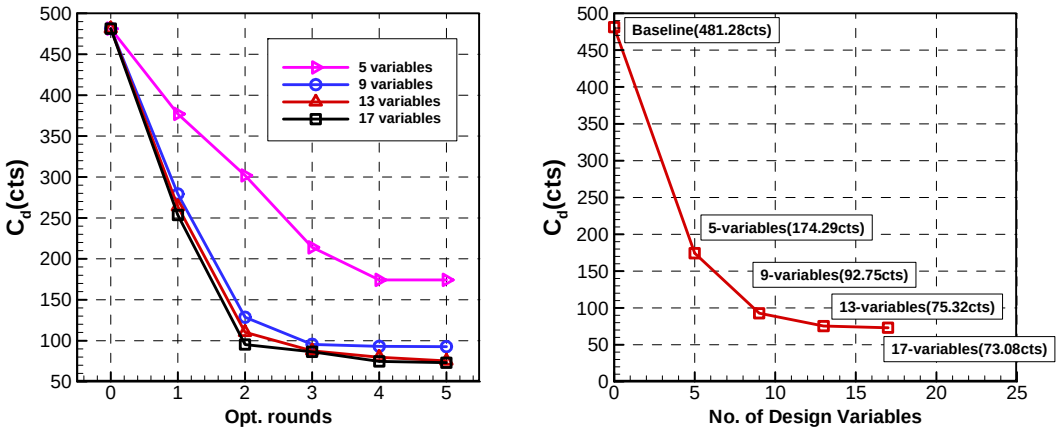

Figure 14. Convergence history (left) and optimization results (right) with different No. of design variables (NACA 0012 airfoil test case)

Table 9. Optimization results with different No. of design variables (NACA 0012 airfoil test case)

No. of design variables	Baseline	5	9	13	17
C_d (cts)	481.28	174.29	92.75	75.32	73.08
N_CFD	/	369	806	795	932

IV. Benchmark Case II: Drag Minimization of RAE 2822 in Transonic Viscous Flow

A. Problem Statement

The optimization problem of this part is the drag minimization of the RAE 2822 airfoil at a freestream Mach number of 0.734 and lift coefficient of 0.824, and Reynolds number of 6.5×10^6 with respect to an area and pitching moment constraints. It can be written as a standard nonlinear programming problem

$$\begin{aligned} \min\ & C_d \\ s.t.\ & C_l = 0.824 \\ & C_m \geq -0.092 \\ & Area \geq Area_{\text{initial}} \end{aligned} \tag{5}$$

where C_m is the moment coefficient and A is the non-dimensional airfoil cross-sectional area.

B. Grid Convergence Study for Initial Airfoil

The grid study for RAE 2822 airfoil uses a special technique called conformal transformation to make sure very good uniformity and orthogonality. And Table 10 shows the grid convergence study for the initial airfoil. It is observed that the difference in lift coefficients of RAE 2822 is converging within 0.1counts and the difference in drag coefficients is converging within 1.0 count gradually with the increase of the number of cells. And the typical grids used for optimization have 512 points in the stream-wise direction and 256 points in the direction normal to the airfoil surface.

Table 10. Grid convergence study for the RAE 2822 with PMNS2D.

Grid size	C_l (cts)	C_d (cts)
192 × 96	82.3	221.66
256 × 128	82.4	208.10
320 × 160	82.4	201.85
384 × 192	82.4	198.65
448 × 224	82.4	196.53
512 × 256	82.4	195.02
576 × 288	82.4	194.09

C. Results

First of all, this results are based on 18 design variables (the order of parameterization is 8), and we conduct an optimization with a global search in an appropriately enlarged design space which is obtained by expanding the initial parameters of baseline 1.5 times and narrowing it by half. In the first round, the allowable number of CFD call is set as 250, and the optimization is convergent when the drag coefficient doesn't decrease anymore. Figure 15 shows the initial design space and the optimal airfoil in the first round. Just as the NACA0012 case, we would like to carry on a multi-round optimization to find a global optimal solution. However, to make the first-round optimization convergent sufficiently, a local search based on the current optimal airfoil is continued in the same design space. Then the first-round optimization terminates, and a quite good result has been found, while the optimal airfoil still has some parameters reaching the boundary of the design space. So the second-round of optimization is conducted. Since we know that the current optimal airfoil is close to the global optimal solution, because the shock on the upper surface is nearly smoothed out in Figure 18, we started with a smaller design space in the second-round optimization. But the optimization is still too difficult to find a slightly better result. So we finally make a local optimization in this smaller design space, and a better result is found with all parameters inside the design space. Until now, the whole optimization terminates, and the optimal solution in the last–round optimization is considered as our global optimum for this case.

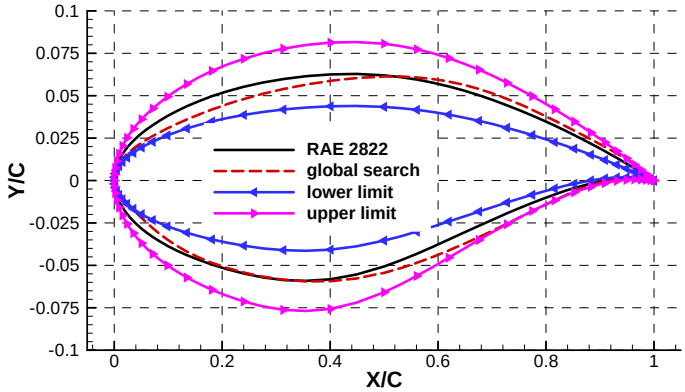

Figure 15. The initial design space and optimal airfoil in the first round for RAE2822 test case.

Figure 16 shows the convergence histories of the optimizations. The force coefficients and constraints of the optimal airfoil in each round are shown in Table 11. And the total cost for global optimization is 592 CFD calls. Figure 17 and Figure 18 shows the comparisons of airfoils and pressure coefficient distributions between the RAE 2822 and the optimal airfoils. The comparison of pressure coefficient contours for baseline and final optimal airfoils are shown in Figure 19. As we can see, the three optimal airfoils are extremely close in shape, and the shock intensity is decreased sharply. Their pressure coefficient distributions have slightly difference at the shock location

and the pressure coefficient distribution of the final optimal airfoil (local search2) has the smallest fluctuation leading to its minimum drag coefficient. In addition, the pressure coefficient distribution of final optimal airfoil has the double-shock structure which is beneficial to reduce the drag.

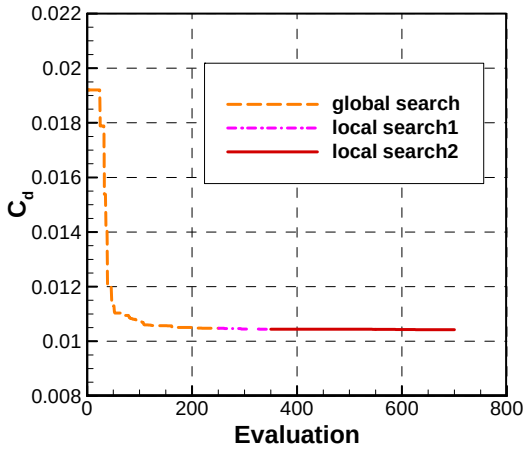

Figure 16. Convergent history of drag coefficient in multi-round optimization (RAE2822 test case).

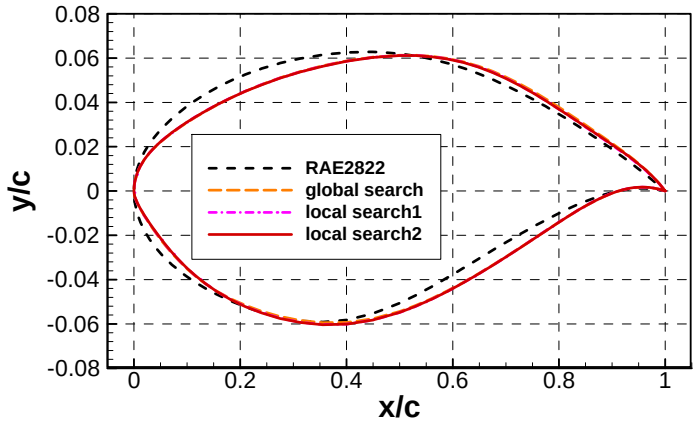

Figure 17. Shape of optimal airfoils in each round of optimization (RAE2822 test case).

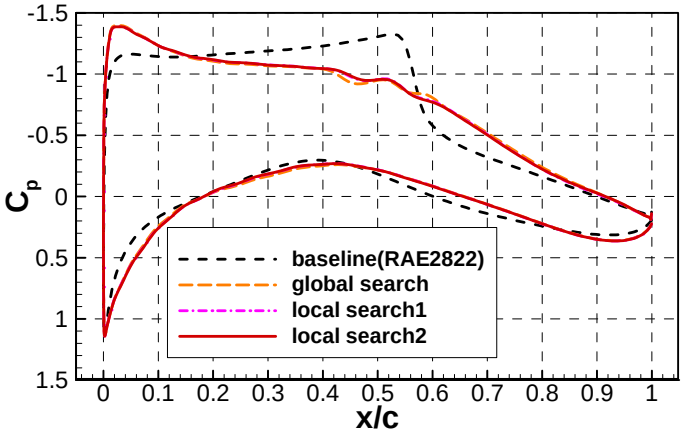

Figure 18. Pressure coefficient distributions of optimal airfoils in each round of optimization (RAE2822 test case).

Table 11. Force coefficients and constraints of optimal airfoil in each round (RAE2822 test case).

Variable	Baseline	1st round Global Opt.	1st round Local Opt.	2nd round Local Opt.
C_l (cts)	82.4	82.5	82.4	82.4
C_d (cts)	195.02	104.80	104.42	104.27
$C_{m,c/4}$	-0.092129	-0.089556	-0.088022	-0.088016
A	0.07794	0.07795	0.07794	0.07794
N_CFD	/	219	97	276

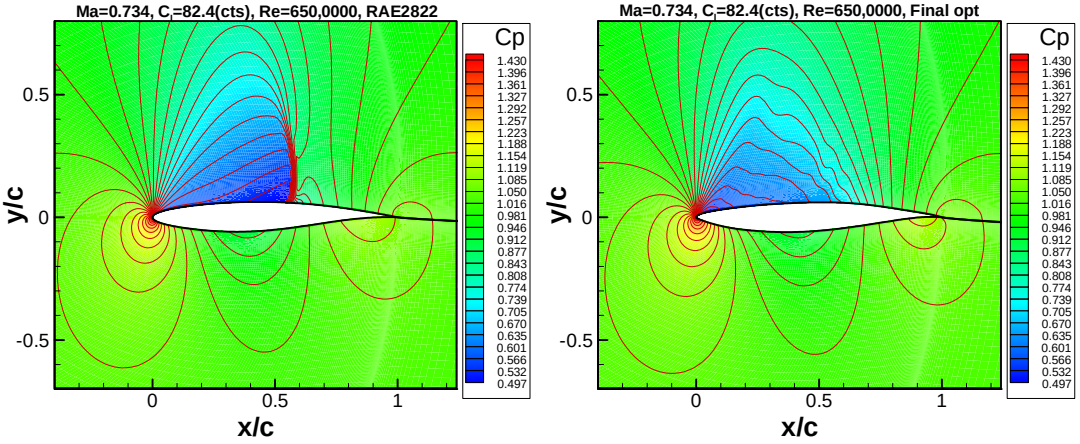

Figure 19. Comparison of pressure coefficient contours of baseline and final optimum airfoils (RAE2822 test case).

D. Grid Convergence Study for the Optimum Airfoil

The grid study for the final optimal airfoils is presented in Table 12. The far-field distance is set as 90 chord lengths away from the airfoil surface. It is shown that the difference in drag coefficients is converging within 1.0 count with the increase of the number of grid cells.

Table 12. Grid convergence study for the final optimal airfoil (local search2) with PMNS2D.

Grid size	C_l (cts)	C_d (cts)
192 × 96	82.4	127.75
256 × 128	82.4	113.99
320 × 160	82.4	108.92
384 × 192	82.4	106.58
448 × 224	82.4	105.21
512 × 256	82.4	104.29
576 × 288	82.4	103.62
640 × 320	82.4	102.98

E. The impact of dimensionality of design space

To study the impact of the dimensionality on the optimization results as well as the computational costs, the order of the parameterization are set as 4, 6, 8, 10 (for CST parameterization), and the actual number of design variables is 10, 14, 18, 22 which means 5, 7, 9, 11 design variables on the upper and lower surface respectively. The same methodology has been applied for the optimization with different number of design variables. The comparisons of airfoils and pressure distributions of the optimal airfoils with different dimensions are shown in Figure 20 and Figure 21.

It is observed that the optimization with varying number of design variables results in different design, there are certain differences between the shape and the pressure distribution of the optimal airfoils. However, because the

shock on the upper surface is nearly smoothed out, the drag coefficients of the optimal airfoils are close in Figure 22. The results show that the optimal solution is insensitive to the number of design variables with CST method to parameterize the airfoils in this problem. And in order to improve the efficiency of the optimization, ten variables are enough to come to a good result.

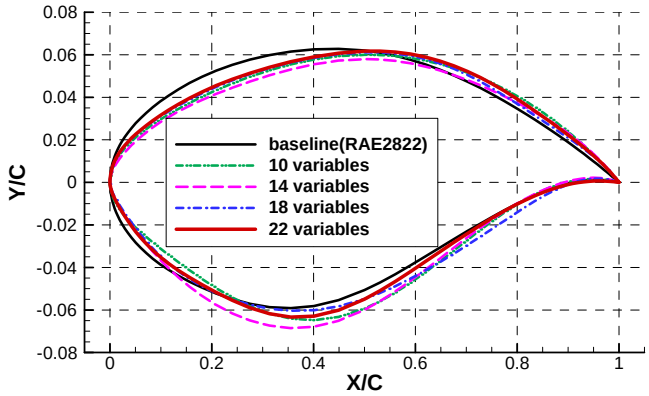

Figure 20. Shape of optimal airfoils with different No. of design variables (RAE2822 test case).

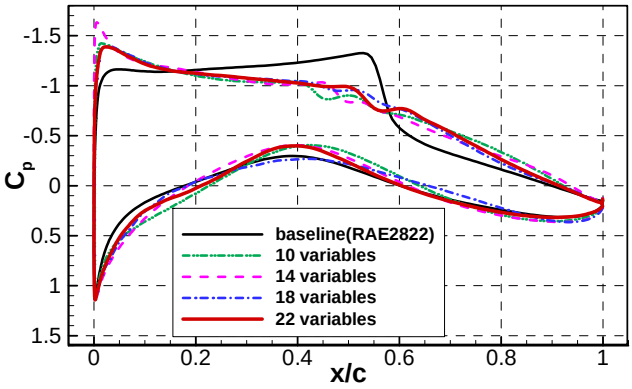

Figure 21. Pressure coefficient distributions of optimal airfoils with different No. of design variables (RAE2822 test case).

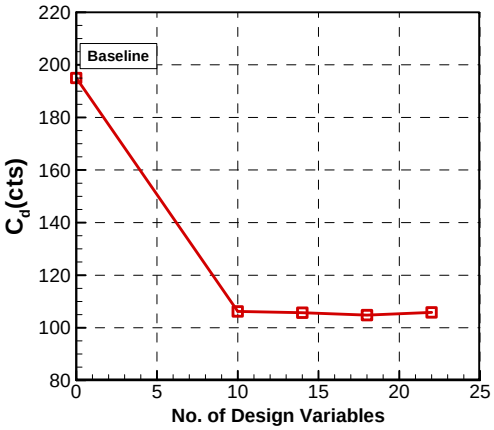

Figure 22. Optimization results with different No. of design variables (RAE2822 test case).

V. Conclusion

In this work, a surrogate-based multi-round optimization strategy is used to find the global optimal solutions of two aerodynamic optimization benchmark problems. The results show that this method is suitable for global optimization and quite good results are found in both the optimization problems of NACA0012 case and RAE2822 case. The results has been compared with that of the gradient-based method[36], which shows that better results can be obtained by surrogate-based optimization method. The impact of dimensionality is also studied, and we find that the optimal solution is quite relevant to the dimension of design space in the NACA 0012 drag minimization problem, and as the dimension of the design space increases, the optimal design monotonically improves, and gradually approaches a limit value; however, for the RAE2822 drag minimization problem, the optima is insensitive to the dimensions. Note that the conclusions are only valid when CST method is employed. Our multi-round optimization strategy can be viewed as an optimization method with manually room-in the design space and refine the design space, and the optimization method with self-adaptive design space combined with trust-region method is valuable for further investigation in the future.

Acknowledgments

This research was supported by "the National Natural Science Foundation of China (NSFC)" under grant No. 1 1272265 and by “the Fundamental Research Funds for the Central Universities".

The author would like to thank Dr. Jun Liu for providing technical support of the optimization code.

References

[1]Reuther, J., Jameson, A., Farmer, J., Martinelli, L. and Saunders,D., “Aerodynamic shape optimization of complex aircraft configurations via an adjoint formulation,” AIAA paper 96-0094, January 1996.

[2]Brezillon, J. and Gauger, N. R., “2D and 3D Aerodynamic Shape Optimization using the Adjoint Approach,” *Aerospace Science and Technology*, Vol. 8, No. 8, 2004, pp. 715-727.

[3]Laurenceau, J., Meaux, M., Montagnac, M. and Sagaut, P., “Comparison of Gradient-Based and Gradient-Enhanced Response-Surface-Based Optimizers,” *AIAA Journal*, Vol. 48, No. 5, 2012, pp. 981-994.

[4]Jameson, A., “Aerodynamic design via control theory,” *Journal of Scientific Computing*, Vol. 3, No. 3, 1988, pp. 233-260.

[5]Jameson, A., “Optimum aerodynamic design using CFD and control theory,” AIAA paper 95-1729, June 1995.

[6]Queipo, N. V., Haftka, R. T., Shyy, W., Goel, T., Vaidyanathan, R. and Tucker, P. K., “Surrogate-based analysis and optimization.” *Progress in Aerospace Sciences*, Vol. 41, 2005, pp. 1-28.

[7]Audet, C., Dennis, J. E., Moore, D. W., Booker, A. and Frank P. D., “A Surrogate-Model-Based Method For Constrained Optimization,” AIAA paper 2000-4891, 2000.

[8]Jonsson, E., Leifsson, L. and Koziel, S., “Aerodynamic Optimization of Wings by Space Mapping,” AIAA paper 2013-0780, 2013.

[9]Simpson, T. W., Toropov, V., Balabanov, V. and Viana, F.A.C., “Design and analysis of computer experiments in multidisciplinary design optimization: a review of how far we have come - or not,” AIAA paper 2008-5802, 2008.

[10]Giunta, A. A., Wojtkiewicz, S. F. and Eldred, M. S., “Overview of modern design of experiments methods for computational simulations,” AIAA paper 2003-649, 2003.

[11]Parr, J. M., Keane, A. J., Forrester, A. I. J. and Holden, C. M. E., “Infill sampling criteria for surrogate-based optimization with constraint handling,” *Engineering Optimization*, Vol. 44, No. 10, 2012, pp. 1147-1166.

[12]Jones, D. R., Schonlau, M. and Welch, W. J., “Efficient Global Optimization of Expensive Black-Box Functions,” *Journal of Global Optimization*, Vol. 13, No. 4, 1998, pp. 455-492.

[13]Forrester, A. I. J., Keane, A. J., “Recent advances in surrogate-based optimization,” *Progress in Aerospace Sciences*, Vol. 45, 2009, pp. 50-79.

[14]Liu, J., Han, Z. H. and Song, W. P., “efficient Kriging-Based Aerodynamic Design of transonic Airfoils: some key issues”, AIAA paper 2012-0967, 2012.

[15]Song, W., Keane, A. J., “Surrogate-Based Aerodynamic Shape Optimization of a Civil Aircraft Engine Nacelle,” *AIAA Journal*, Vol. 45, No. 10, 2007, pp. 2565-2574.

[16]Box, G. E. P., Drapper, N. R., “Empirical Model Building and Response Surfaces,” *Journal of the Royal Statistical Society*, 1987.

[17]Lancaster, P., Salkauskas, K., “Surfaces generated by moving least squares methods,” *Mathematics of Computation*, Vol. 37, No. 155, 1981, pp. 141-158.

[18]Broomhead, D. S., Lowe, D., “Multi-variable functional interpolation and adaptive networks,” *Proceedings Ijcai*, Vol. 2, No. 3, 1988, pp. 321-355.

[19]Krige, D. G., “A statistical approach to some basic mine valuation problems on the Witwatersrand” *Journal of the Chemical, Metallurgical and Mining Society of South Africa*, Vol. 94, No. 3, 1951, pp. 95-111.

[20]Sacks, J., Welch, W. J., Mitchell, T. J. and Wynn, H. P., "Design and Analysis of Computer Experiments," *Statistical Science*, Vol. 4, 1989, pp. 409–423.
[21]Forrester, A. I. J., Sóbester, A., Keane, A. J., "Engineering Design via Surrogate Modelling - A Practical Guide," *Progress in Astronautics and Aeronautics Series*, 226, published by John Wiley & Sons, 2008.
[22]Vapnik, V. N., "The Nature of Statistical Learning Theory," Springer Berlin, 2000.
[23]Zhang, K. S., Han, Z. H., "Support Vector Regression-based Multidisciplinary Design Optimization in Aircraft Conceptual Design," AIAA paper 2013-1160, 2013.
[24]Han, Z. H., "Improving Adjoint-based Aerodynamic Op-timization via Gradient- Enhanced Kriging," AIAA paper 2012-0670, 2012.
[25]Chung, H. S., Alonso, J. J., "Using gradients to construct cokriging approximation models for high-dimensional design optimization problems," AIAA paper 2002-0317, 2002.
[26]Han, Z. H., Zimmermann, R. and Goertz, S., "an Alter-native Cokriging Model for Variable-Fidelity Surrogate Modeling," *AIAA Journal*, Vol. 50, No. 5, 2012, pp. 1205-1210.
[27]Han, Z. H., and Goertz, S., "Hierarchical Kriging Model for Variable-Fidelity Surrogate Modeling," *AIAA Journal*, Vol. 50, No. 5, 2012, pp. 1285-1296.
[28]Kennedy, M. C. and O'Hagan, A., "Predicting the Output from a Complex Computer Code When Fast Approximations Are Available," *Biometrika*, Vol. 87, 2010, pp. 1–13.
[29]Alexandrov, N., Dennis, J. E., Lewis, R. M. and Torczon, V., "A trust-region framework for managing the use of approximation models in optimization," *Structural Optimization*, Vol. 15, 1998, pp. 16-23.
[30]Jones, D. R., "A Taxonomy of Global Optimization Methods Based on Response Surfaces," *Journal of Global Optimization*, Vol. 21, No. 4, 2001, pp. 345-383.
[31]Kumano, T., Jeong, S., Obayashi, S., Ito, Y., Hatanaka, K. and Morino, H., "Multidisciplinary Design Optimization of Wing Shape for A Small Jet Aircraft Using Kriging Model," AIAA paper 2006-932, 2006.
[32]Kanazaki, M., Imamura,T., Jeong, S. and Yamamoto, K., "High-Lift Wing Design in Consideration of Sweep Angle Effect Using Kriging Mode," AIAA paper 2008-175, 2008.
[33]Kulfan, B. M., "Universal Parametric Geometry Representation Method," *Journal of Aircraft*, Vol. 45, No. 1, 2008, pp. 142–158
[34]Xie, F., Song, W. P. and Han, Z. H., "Numerical Study of High-Resolution Scheme Based on Preconditioning Method," *Journal of Aircraft*, Vol. 46, No. 2, 2008, pp. 520-525.
[35]Han, Z. H., He, F., Song, W. P. and Qiao, Z. D., "A Preconditioned Multigrid Method for Efficient Simulation of Three-dimensional Compressible and Incompressible Flows," *Chinese Journal of Aeronautics*, Vol. 20, No. 4, 2007, pp. 289–296.
[36]Tesfahunegn, Y. A., Koziel, S., Gramanzini, J. R., Hosder, S., Han, Z. H. and Leifur L. "Application of Direct and Surrogate-Based Optimization to Two-Dimensional Benchmark Aerodynamic Problems: A Comparative Study," AIAA paper 2015-0265, 2015.